Applied Catalysis B: Environmental 250 (2019) 99–111

Contents lists available at ScienceDirect

Applied Catalysis B: Environmental

journal homepage: www.elsevier.com/locate/apcatb

Co-aromatization of methane with propane over Zn/HZSM-5: The methane reaction pathway and the effect of Zn distribution

Peng He[a], Jack S. Jarvis[a], Shijun Meng[a], Qingyin Li[a], Guy M. Bernard[b], Lijia Liu[c], Xiaohui Mao[d], Zhao Jiang[e], Hongbo Zeng[d], Vladimir K. Michaelis[b], Hua Song[a,*]

[a] Department of Chemical and Petroleum Engineering, University of Calgary, 2500 University Dr NW, Calgary, Alberta, T2N 1N4, Canada
[b] Department of Chemistry, University of Alberta, 11227 Saskatchewan Drive, Edmonton, Alberta, T6G 2G2, Canada
[c] Jiangsu Key Laboratory for Carbon-Based Functional Materials & Devices, Institute of Functional Nano and Soft Materials (FUNSOM), Soochow University, Suzhou, Jiangsu, 215123, China
[d] Department of Chemical and Materials Engineering, University of Alberta, 9211-116 Street NW, Edmonton, Alberta, T6G 1H9, Canada
[e] School of Chemical Engineering and Technology, Xi'an Jiaotong University, Xi'an, Shaanxi, 710049, China

ARTICLE INFO

Keywords:
Methane co-aromatization
^{13}C isotope labeling
Solid-state NMR
STXM image
Theoretical calculations

ABSTRACT

The co-aromatization of methane with propane is investigated using Zn/HZSM-5 as the catalyst at 400 °C. The presence of methane has a pronounced effect on the product distribution in terms of improved formation of phenyl rings and substitution groups of aromatic species. Isotopic labeling and solid-state NMR spectroscopy studies reveal that the favored site for methane incorporation varies at different stages along the co-aromatization reaction, from the benzylic sites at the initial stage to the phenyl rings and then substitution groups as the reaction proceeds. SIMS spectroscopy of the involved reaction intermediates suggests the formation of C_4 species over the Zn sites that are bonding to the oxygen atoms of the zeolite framework, which is supported by theoretical calculations. The interaction between Zn species and the zeolite framework is also confirmed by XAS and changes in coordination environments are identified through XANES and solid-state NMR spectroscopy. The redistribution of Zn during the reaction is observed on the surface of the zeolite support. Scanning transmission X-ray microscopy images show that Zn is rich in the inner pores compared with the external surface of the catalyst particles in the pristine catalysts. XANES and XPS spectra demonstrate that the Zn concentration increases on the external surface after the reaction, a conclusion that is further supported by the theoretical study. The Zn redistribution might be among the reasons for methane participation pathway alternation during the co-aromatization, since the Zn species located within the inner pores and on the external surface might prefer to catalyze the methane incorporation to the phenyl rings and substitution groups of the formed aromatics, respectively.

1. Introduction

Catalytic transformation of methane, the principal component of natural gas, into more valuable carbon-containing products has provided an effective alternative for the use of natural gas. However, the inert structure of methane impedes its conversion into more value-added chemicals and fuels. In its current utilization scenario, methane must follow multistep conversion strategies via syngas and/or methanol before it can be transformed into higher hydrocarbons, resulting in increased costs and impeding its commercial potential. In 2017, the price of Henry Hub natural gas averaged US $3.10 per million British thermal units (MBTU), while that of the West Texas Intermediate (WTI) light sweet crude oil averaged US $50.8 per barrel, which equates to US $9.15 per MBTU. The greatly underutilized value of methane has driven researchers to investigate methods that can potentially boost the profitability of the natural gas industry; the necessity of this goal is highlighted given the current era of low energy prices. The conversion of low cost methane into high value commodities including more commercially useful chemicals and liquid fuels has attracted special attention but due to its symmetric molecular structure, methane activation presents a great challenge for the entire catalysis field. Oxidative coupling of methane to convert it into more valuable chemicals such as ethylene and methanol has been extensively studied [1–5]. Nonetheless, an increased methane conversion often comes with a loss in selectivity due to the production of CO and CO_2 as well as the more prominent reactivity of desired products compared with methane,

* Corresponding author.
E-mail address: sonh@ucalgary.ca (H. Song).

https://doi.org/10.1016/j.apcatb.2019.03.011
Received 23 December 2018; Received in revised form 1 March 2019; Accepted 2 March 2019
Available online 04 March 2019
0926-3373/

resulting in a significantly reduced yield of the desired products. The direct transformation of methane into liquid chemicals such as aromatics has been explored under non-oxidative environments over the last few decades [6–12]. This is more valuable for the petrochemical industry, but the commercialization of this process is significantly impeded by even lower product yields and high reaction temperatures, which are often above 700 °C. Nevertheless, the conversion of methane at lower temperatures (400–600 °C) is significantly enhanced when co-fed with hydrocarbons [13–19]. Among the co-fed hydrocarbons, propane represents an abundant feedstock with promising commercial potential. As a product from the petroleum industry, whose application is often limited to residential heating systems and stoves, the aromatization of propane has drawn great attention recently [20–24].

The aromatization activity of light alkanes, including methane, over Zn-modified zeolite catalysts under non-oxidative conditions has been studied in recent decades because of their good catalytic capacity [24–27] with a lot of effort being focused on the activation mechanism of methane over these catalysts. The activation of the methane C—H bond can be witnessed even at room temperature [28], with the adsorption of methane on the Zn modified zeolites resulting in the observation of signals assigned to Zn-CH_3 species [29–31] and O-CH_3 species [31]. Besides the activation of pure methane, the co-reaction mechanism between methane and other hydrocarbons has also been explored. Luzgin et al. [31] observed that methane is incorporated into the phenyl rings to form methyl groups during the co-aromatization of methane and propane. It is proposed that when co-fed with higher hydrocarbons, methane is activated and then attached to aromatic species as methyl groups before it is transferred to the phenyl rings. These mechanistic studies, however, are often carried out under vacuum, which may differ from the real reaction conditions for potential commercial applications.

The co-aromatization of methane with higher hydrocarbons such as propane in this work is closely related to the surface Zn species as the catalytic active site. Gabrienko et al. [32] investigated the methane activation capacity of Zn^{2+} and ZnO species through H/D exchange reactions; solid-state nuclear magnetic resonance (SSNMR) spectra were acquired upon the adsorption of methane and the mixture of methane and benzene on the catalysts. It is reported that the nature of Zn species, such as isolated Zn^{2+} or ZnO clusters, imposes a pronounced impact on the methane participation efficiency, where the Zn^{2+} species is more effective at methane activation. Therefore, it is necessary to probe the chemical environment of Zn species in the catalyst and achieve a better understanding of the catalytic performance during the co-aromatization of methane and propane. Among the techniques used to characterize solid materials, SSNMR is a particularly powerful tool to sensitively probe the chemical environment of Zn species [33,34]. Qi et al. [35] investigated the synergic effect between Brönsted acid sites and Zn species using ^{67}Zn-enriched precursors. It is reported that the dispersed ZnO particles on ZSM-5 result in the lack of quadrupolar line shape, maintaining a high degree of local symmetry (e.g., pseudo-tetrahedral). The only NMR-active stable isotope of zinc is quadrupolar ^{67}Zn, which makes the acquisition of high-quality SSNMR spectra challenging because of its quadrupole moment (150 mb), low γ (1.6767 rad·T^{-1}·s^{-1}, 6.3% of the ^{1}H value), and low natural abundance (4.1%) [36]. Considering these challenging NMR properties, it is more favorable to execute the ^{67}Zn SSNMR spectroscopy study under an ultrahigh magnetic field (21.1 T) and isotopic enrichment. A preliminary assessment of potential Zn chemical environments is performed at 21.1 T at natural abundance.

The effect of catalytic site distribution on the catalytic reaction pathway has attracted attention. Kosinov et al. [37] studied the conversion of CH_4 to benzene over Mo/HZSM-5 at 700 °C and attributed the aromatization capacity to the MoC_x species dispersed in the micropores of ZSM-5. However, understanding the function of the sites located on the inner and external pores is challenging. Ding et al. [38] investigated the effect of silanation of external acid sites on the product selectivity during CH_4 aromatization over Mo/HZSM-5. It was observed that the selectivity of large aromatic molecules is decreased if the preferred catalytic sites are located in the inner pores, where the bimolecular reaction and transition-state formation are suppressed by spatial constraints. The authors have investigated the effect of the location of Ag and Ga species on the co-aromatization of methane and olefins [39]. When the active Ag and Ga sites are loaded in the inner pores of ZSM-5, the participation of methane in phenyl ring formation is favored. The Ag and Ga sites on the external surface are more effective in catalyzing the incorporation of methane to the branch groups in the aromatic products. When modified by Zn, the Brönsted acid sites (bridging OH groups) in the zeolite framework may be consumed to stabilize the Zn species, resulting in decreased Brönsted acid site number and increased Lewis acid site number [25,40,41]. The change of Lewis and Brönested sites might exert critical impacts on the catalytic performance in terms of propane conversion, product selectivity and BTX yield [41]. The Brönsted site may activate the alkane molecule and remove one H atom, while another H is transferred to the zeolite oxygen to produce an alkene molecule [42]. The Zn site may bond to the carbon atom of propane while transferring a hydrogen atom from this carbon atom to an oxygen site of the zeolite framework [43]. When Zn migrates from the inner pores to the external surface, there may be stronger Brönsted acidity in the inner pores and stronger Lewis acidity on the external surface, which could impose an impact on the reaction pathway in the aromatization process.

Differentiating the metal species located in different locations of the zeolite framework presents a challenging task due to the difficulty in the quantification of metal species within the inner pores compared with that on the external surface. X-ray photoelectron spectroscopy (XPS) could detect the oxidation state and quantify the concentration of designated elements in the catalysts, but its application is only limited to the atoms exposed on the external surface. Nevertheless, X-ray absorption spectroscopy (XAS) has been engaged to investigate the element distribution in solid materials. In X-ray adsorption near edge structure (XANES) spectra, the total electron yield (TEY) is due to the elements on the surface of the solid sample, while the total fluorescence yield (TFY) is attributed to the elements within the bulk below the surface [44]. Therefore, it is possible to investigate the chemical environment and concentration of the elements within the inner pores and on the external surface. Moreover, by acquiring XANES spectra of various small sections (10–20 nm) of the catalyst, scanning transmission X-ray microscopy (STXM) provides an excellent combination of chemical speciation and microscopy with a high spatial resolution, which can be employed as a powerful tool to examine the spatial distribution of metals including Zn species on the catalyst.

Thus, this paper systematically studies the participation of methane during co-aromatization with propane over Zn/HZSM-5. The products are analyzed by gas chromatography-mass spectrometry (GC–MS) and compared with its N_2 reaction counterpart to ascertain the contribution of methane in the co-aromatization process. The participation of methane is further confirmed by ^{13}C isotope labeling and SSNMR studies. Secondary ion mass spectrometry (SIMS) is employed to probe the reaction intermediates. ^{27}Al and ^{67}Zn SSNMR, XAS and XPS reveal the chemical environment of the Zn species, whose redistribution over the reaction is demonstrated by comparing the XANES, STXM and XPS spectra of the catalysts collected before and after the reaction.

2. Experimental

2.1. Synthesis of catalysts

Ammonium type ZSM-5 (NH_4-ZSM-5) with a SiO_2/Al_2O_3 ratio of 23:1 was obtained from Zeolyst USA. NH_4-ZSM-5 was converted into HZSM-5 by calcination at 600 °C in ambient air for 3 h. The metal-modified HZSM-5 was prepared using the wetness impregnation method. 0.13 g $Zn(NO_3)_2{\cdot}6H_2O$ (98%, Alfa Aesar) salt was dissolved in

10 g deionized (DI) water to form the aqueous solution of the metal precursors, which was then impregnated into 10 g HZSM-5 to obtain 5% Zn/HZSM-5. The obtained wet powder was dried in the oven at 92 °C overnight, followed by calcination at 600 °C for 2 h in ambient air.

2.2. Catalytic performance evaluation

The co-aromatization reactions were carried out in a 100 mL batch reactor manufactured by the Parr Instrument Company which is capable of tolerating temperatures up to 500 °C and pressures up to 35 MPa. The diameter and length of the reactor cylinder are 5 and 12 cm, respectively. In a typical run, 0.1 g catalyst was placed at the bottom of the reactor cylinder. The reactor was sealed, purged with propane (99.5%, Praxair) and then pressurized to an absolute pressure of 2 atm by propane. The reactor was then pressurized to 5.0 MPa with methane (99.97%, Praxair). N_2 (99.998%, Praxair) was also used to pressurize the reactor in control group reactions. The reactor temperature was then ramped up at a rate of 20 °C/min to the target temperature and held for a designated time. Upon reaction completion, the reactor was put in cold water to quickly cool to room temperature before product collection. The gas product was discharged to a 2.2 L cylinder, which was previously purged with N_2. The temperature and pressure (250–350 kPa) were recorded before the gas product was analyzed by micro-gas chromatography. The formed liquid product embedded into the charged solid catalyst was extracted using 10.0 g CS_2 (99.9%, Sigma) as the solvent and internal standard for ensuing NMR analysis of each batch of reaction.

Reactions between propane and $^{13}CH_4$ (99.9% ^{13}C, Cambridge Isotope Laboratories Inc., Tewksbury, MA, USA) were conducted in a similar manner when 0.1 g catalyst was charged. The reactor was pressurized to 500 kPa by $^{13}CH_4$ after the reactor was purged and filled with 200 kPa propane. The reactor was then pressurized to 5.0 MPa using non-isotopic labeled CH_4 before conducting the reaction.

The composition of the product oil was determined by a pre-calibrated Gas Chromatography-Mass Spectrometer (GC–MS: PerkinElmer GC Claus 680 and MS Clarus SQ 8 T) equipped with a Paraffins-Olefins-Naphthenes-Aromatics (PONA) column (Agilent HP-PONA). The oven temperature of the GC was programmed to hold at 35 °C for 15 min, ramp to 70 °C at 1.5 °C/min, rise to 150 °C at 3 °C/min and hold for 30 min, then ramp to 250 °C at 3 °C/min and hold for 2 min. The GC–MS peak areas were calibrated using standard compound spectra to correlate the peak areas with the moles of the compounds.

The average carbon number of product molecules is calculated based on the molar fraction of product molecules with variable carbon numbers. The molar fraction (y_i) of each molecule with a formula of C_pH_q in the molecule matrix is obtained by GC–MS analysis of the products. The average carbon number is calculated by:

$$Average\ Carbon\ Number = \sum (p_i \times y_i)$$

The substitution index demonstrates the fraction of carbon atoms that are attached to substituent groups among the phenyl ring carbon atoms in the product molecule matrix. The molar fraction (y_i) of each molecule, which has *m* carbons atoms on the phenyl rings along with *n* carbon atoms on substitution groups, is obtained by GC–MS analysis of the products. The substitution index is calculated by

$$Substitution\ Index = \sum \left(\frac{n_i}{m_i} \times y_i\right)$$

The aromatic carbon fraction is the fraction of carbon atoms on the phenyl rings among all the carbon atoms in the product matrix. The molar fraction (y_i) of each molecule, which has *m* carbon atoms on the phenyl rings and *n* carbon atoms on the substitution groups, is obtained by GC−MS analysis of the products. The aromatic carbon fraction is calculated by

$$Aromatic\ carbon\ fraction = \sum \left(\frac{m_i}{m_i + n_i} \times y_i\right)$$

2.3. Sample characterization

^{13}C and ^{27}Al magic-angle spinning (MAS) SSNMR spectra were acquired at 11.75 T ($\nu_0(^{13}C)$ = 125.8 MHz; $\nu_0(^{27}Al)$ = 130.4 MHz) on a Bruker Avance 500 NMR spectrometer using a Bruker MAS probe operating in double-resonance mode (University of Alberta). Samples were packed in 4.0 mm outer diameter zirconia rotors. ^{13}C cross-polarization (CP) MAS NMR spectra were acquired by setting the spinning frequency to 8.5 kHz to ensure that spinning sidebands did not overlap with peaks of interest. ^{13}C data were referenced with respect to TMS by setting the high-frequency ^{13}C peak of adamantane to 38.56 ppm [45]. The $\pi/2$ pulse was 4 μs, the contact time was 3 ms, the recycle delay was 3 s and between 20k and 30k transients were co-added for each ^{13}C NMR spectrum. ^{27}Al MAS NMR experiments were acquired with a spinning frequency of 14 kHz. ^{27}Al data were referenced with respect to 1.0 M $AlCl_3$ (aq) (δ = 0 ppm) [46]. The $\pi/2$ pulse was 1.33 μs, the recycle delay was 1 s and the number of co-added transients ranged from 1k to 4k.

^{67}Zn non-spinning SSNMR spectra were acquired at 21.1 T (ν_0 = 56.3 MHz) on a Bruker Avance II 900 NMR spectrometer using a home-built 7 mm HX non-spinning probe (NRC, Ottawa, ON, Canada). Spectra were acquired using a quadrupolar-echo (and CPMG) pulse sequence with 3.0 μs ($\pi/2$) pulse widths and an interpulse delay of 40 μs. For the Zn/HZSM-5 sample, the recycle delay was 0.5 s; 144 K co-added transients were acquired. The contribution from the background Zn metal of the probe was subtracted by acquiring a spectrum without sample (i.e., an empty rotor in the probe) under otherwise identical conditions and subtracting it from that for the sample. Similar experimental conditions were used for the ZnO spectrum, with 4k transients co-added; in this case a background correction was not necessary. Chemical shifts were referenced to a 1.0 M solution of $Zn(NO_3)_2$ (aq) (δ_{iso} = 0.0 ppm) [47].

The time-of-flight secondary ion mass spectrometry (TOF-SIMS) spectra were acquired with Physical Electronics TRIFT V nanoTOF spectrometer equipped with a 30 keV Au^+ pulsed primary ion source in bunched mode. The analysis was carried out in an area of 400 μm x 400 μm. The total ion dose was below 1012 ions/cm^2. Mass spectra were collected in the mass-to-charge range of 0–1850 m/z, for positive polarity and negative polarity. Charge compensation was accomplished using 10 eV electrons.

STXM measurements were conducted at the SM beamline (10ID-1) at the Canadian Light Source (CLS), which is equipped with a 35 nm outermost-zone plate (CXRO, Berkeley Lab). The procedure is similar to that described in reference [48]. The diffraction-limited spatial resolution for this zone plate is 30 nm. Image sequence (stack) scans over a range of photon energies were acquired for the same sample region at the Zn $L_{3,2}$-edge. The STXM data was analyzed using the aXis2000 software package. More details of the sample preparation and STXM measurements are included in the Supporting Information.

The standard Zn $L_{3,2}$-edge XANES measurements were performed at CLS on the high-resolution Spherical Grating Monochromator (SGM) beamline (11ID-1). The SGM beamline uses a 45 mm planar undulator and three gratings to cover a photon energy region from 250 to 2000 eV. It offers a resolution greater than 5000 E/ΔE at energies below 1500 eV [49]. The angle between the incident beam and the sample surface was at normal incidence. Spectra were recorded in the total fluorescence yield (TFY) mode using a solid state detector and the total electron yield (TEY) mode by measuring the sample current with a current amplifier.

The morphologies of zeolites were characterized using a JEOL 2100 transmission electron microscope (TEM) at 200 kV. The element distribution was revealed by energy-filtered TEM (EFTEM) [50], which

images a specimen via inelastically scattered electrons that result in a specific energy loss and inner shell ionization. In this work, the Zn M-shell ionization edge was used to map the Zn element distribution.

2.4. DFT calculations

The DFT calculations were performed using DMol3 [51] in Materials Studio (Accelrys Inc.). Double-numeric quality basis set (DNP) with the gradient-corrected GGA functional of Becke [52] and B3LYP description of exchange and correlation effects [53] were used to optimize the geometry of the molecules. A Fermi smearing of 5×10^{-3} Ha and a real-space cut-off of 4.0 Å was used for the numerical integration. The tolerances of energy, gradient, and displacement convergence were 2×10^{-5} Ha, 4×10^{-3} Ha/Å and 5×10^{-3} Å, respectively.

The structure of Zn/HZSM-5 was optimized first and energies were obtained. The number of Al sites was determined based on the SiO_2/Al_2O_3 molar ratio of 80. Al atoms occupied the T2 and T12 sites in the zeolite framework [54]. The Zn atoms were bonded to the zeolite framework. The charges of the structures were balanced by adding H atoms at the terminal sites on the edges. The catalyst structures in the presence of the organic moiety were further optimized. The energies of isolated atoms were chosen as the zero energy reference.

To identify the effect of zinc position, the energy difference between two zeolite clusters is calculated based on following equation, where E_{outer} is the energy of the cluster with zinc atoms on outer surface and E_{inner} is the energy of the cluster with zinc atoms in the inner pore.

$$\Delta E = E_{Outer} - E_{Inner}$$

3. Results and discussions

3.1. Methane co-aromatization with propane over Zn/HZSM-5

The co-aromatization of methane and propane was carried out at 400 °C for 15 s, 3 min, 9 min, 20 min and 60 min, respectively. The quantified distributions of the obtained aromatic products are shown in Fig. 1 and tabulated in Table S1. The GC−MS spectra of the liquid products obtained from these reactions are displayed in Figure S1. When quenched at a short reaction time in the presence of methane, i.e., 15 s, 3 min and 9 min, the fraction of naphthalene and its derivatives (labeled in Figure S1) is high among the collected liquid products. As the reaction time is extended to 20 and 60 min, their fraction is decreased, whereas the fraction of aromatics with a single phenyl ring and multiple branches, such as xylenes and mesitylene, is increased. The substitution index is increased from 0.167, 0.155 and 0.137 at 15 s, 3 min and 9 min, to 0.218 and 0.204 at 20 and 60 min, while the aromatic carbon fraction is decreased from 0.823, 0.849 and 0.862, to 0.790 and 0.793, respectively (Table S2). The reaction is also executed with only propane under a N_2 environment. The product distribution under N_2 and CH_4 environments are compared and it is observed that methane participation converts some of the benzene, toluene and xylenes to larger molecules. Initially, they are converted to naphthalene derivatives, which is more significant under CH_4. As the reaction continues, more monoaromatics with more or larger substitution groups (C_9 and C_{10+}) are produced due to methane participation.

Upon quenching after 15 s, octane is present in the liquid product, which disappears as the reaction continues. Thus, C_8H_{18} might be a reaction intermediate and the precursor of the aromatic products, a claim supported by the methane and propane co-aromatization product distribution obtained at lowered temperatures, i.e., 350 and 380 °C, and quenched after reaction for 15 s. As shown in Figure S2, not only C_8H_{18} but also C_7H_{16} are of high concentration in the product matrix. When CH_4 is present, the peak intensity due to C_8H_{18} grows stronger compared with that of C_7H_{16}, suggesting that methane may promote the formation of C_8H_{18} species over C_7H_{16}, probably due to its incorporation. After longer reaction time, more methane and propane are converted to aromatics and alkene and alkane products (Table S3). Alkene and alkane molecules such as ethylene, ethane, propylene and butane are also produced in the gas phase (Table S4). Under methane environment, the percentage of butane is increased while percentage of C_2 products is decreased, suggesting methane participation to form larger molecules.

3.2. Methane participation pathway verification

3.2.1. Solid-state NMR study of the catalysts upon reaction

The participation of methane in the co-aromatization reaction was investigated by ^{13}C isotopic labeling studies. ^{13}C-enriched methane was employed as the methane source in the reactions and compared with its non-isotopic labeled counterparts. When $^{13}CH_4$ was introduced, the reactor was first purged and filled with 200 kPa C_3H_8. After that, it was pressurized to 500 kPa using $^{13}CH_4$, and then pressurized to 5.0 MPa with non-isotopic labeled CH_4. The same procedure was carried out in the non-isotopic labeled counterparts, except for that only non-isotopic enriched methane was employed. When the reaction was carried out at 400 °C for 15 s (Fig. 2a), ^{13}C SSNMR indicates that the ^{13}C enrichment in the product matrix was mainly centered at the peak around 31.2 ppm, which is assigned to carbon atoms on the benzylic sites of the product molecules [55], indicating that this is the preferred site of methane incorporation at the initial stage of the reaction. ^{13}C MAS NMR studies of methane activation and its reaction with other hydrocarbons are often acquired with minimal amount of methane at low pressures and temperatures [28–30]. The detected species are probably due to the reaction intermediates and products produced in the early stages of the reaction. The information from the ^{13}C MAS NMR spectra after reacting for 15 s in the present work is consistent with the pathway reported in literature. For instance, Luzgin et al. [31] found that methane formed methyl groups attached to phenyl rings when reacting with propane. In this work, the ^{13}C peak at 128.9 ppm, assigned to carbon atoms of phenyl rings, is enhanced for the ^{13}C-enriched sample, indicating the existence of other reaction pathways that guide methane participation along with methane incorporation to the benzylic sites.

When the reaction time is prolonged to 9 min, at which point GC–MS analysis indicates a pronounced formation of naphthalene and its derivatives under a CH_4 environment compared with its N_2 counterpart, ^{13}C SSNMR indicates significant enhancement of the peaks due to the phenyl for the sample prepared with $^{13}CH_4$ (Fig. 2b); a noticeable but smaller increase in signal is also observed for peaks in the 13 to 40 ppm range, due to the carbon atoms on the sidechain groups. The intensity of the peak at 31 ppm is unchanged, while the peak intensity is increased at 16.8 and 19.6 ppm under the $^{13}CH_4$ condition. These two peaks are assigned to alkyl sidechain carbon atoms that are not directly bonded to phenyl rings. These observations indicate that the enhanced phenyl ring formation under a CH_4 environment might be closely related to methane incorporation into the phenyl rings. When compared with the spectra collected after the 15 s reaction, the ^{13}C enrichment is shifted from the benzylic site (≈ 31 ppm) to the phenyl rings. This phenomenon suggests that the methane might first be incorporated to the phenyl ring at the benzylic sites, which become part of the phenyl rings as the reaction continues.

When the reaction time is further increased to 20 min, enhancement of peaks under $^{13}CH_4$ conditions occurs at both 129 ppm due to phenyl ring carbon atoms and at 17 and 20 ppm due to alkyl sidechain carbon atoms (Fig. 2c). Comparing this spectrum with that obtained after reaction for 9 min (Fig. 2b), the most significant change is that the relative intensity of the peaks at 17 and 20 ppm are greater than those for the non-enriched counterpart. This observation is consistent with GC–MS analysis results (Fig. 1) that show the formation of aromatics with multiple substitution groups is improved under CH_4 compared with its N_2 counterpart after reaction for 20 min. These phenomena show that as the reaction time is extended to 20 min, the alkyl sites

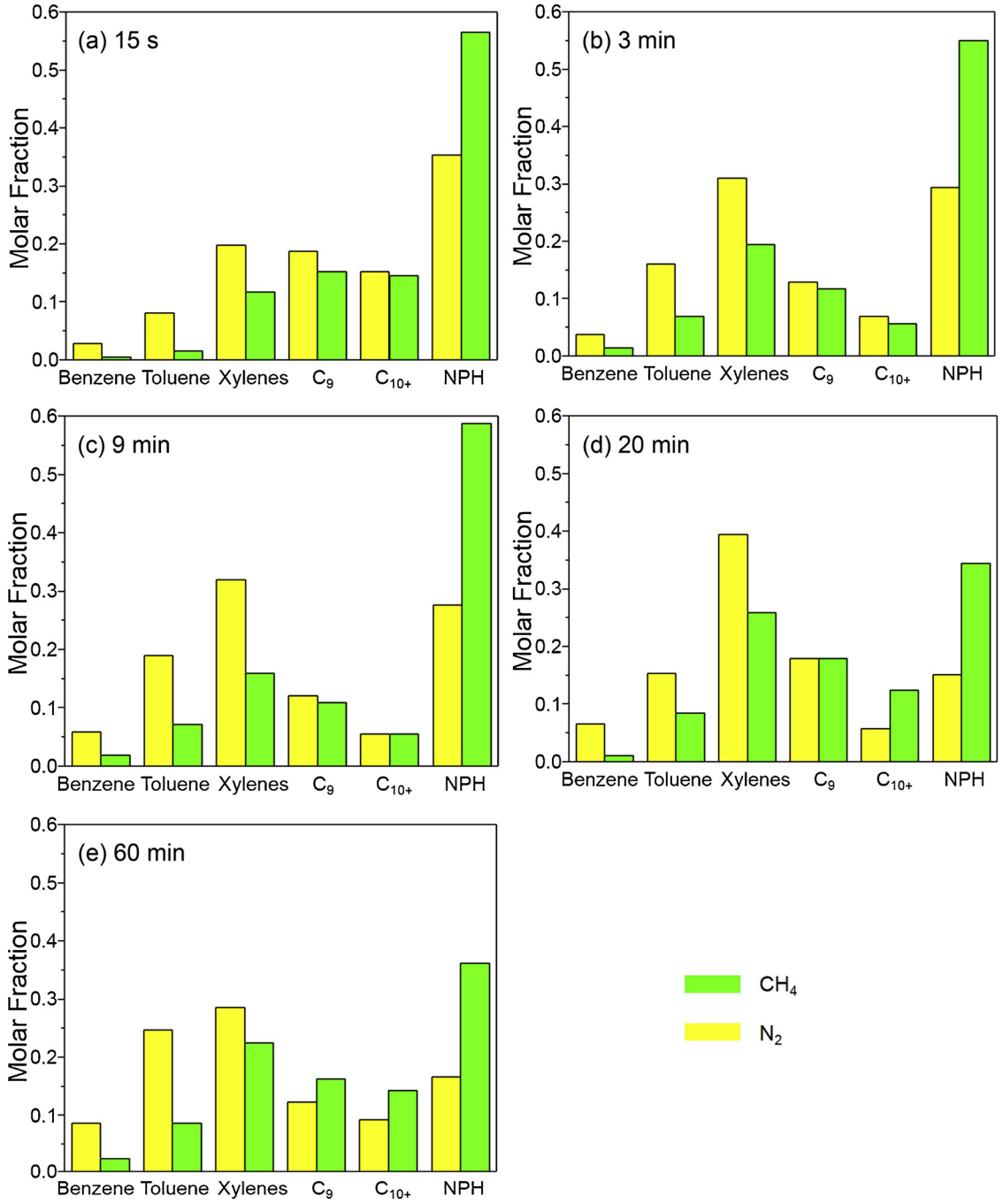

Fig. 1. GC–MS spectra of the products obtained from the co-aromatization of methane with propane and their N_2 counterparts over Zn/HZSM-5 at 400 °C and 5.0 MPa for different reaction times.

rather than the phenyl rings become the preferred sites of methane incorporation.

When these SSNMR spectra are compared with the aforementioned GC–MS spectra, it is observed that initially, methane is incorporated into the benzylic sites of the product molecules. After that, methane starts to participate in the phenyl ring formation, which outpaces the methane incorporation at the benzylic sites. When the reaction proceeds further, methane incorporation to the substitution groups takes precedence over its participation in the phenyl ring formation. It is also worth noting that among all these reaction conditions, the ^{13}C enrichment at 139.5 ppm due to the phenyl ring carbon that is directly bonded to a substitution group does not appear to be significant, suggesting that this site is not among the favored methane incorporation sites.

3.2.2. SIMS study of the catalytic reaction intermediates

To gain a clearer picture of the reaction intermediates formed during the co-aromatization reaction on the catalyst surface, SIMS spectra were obtained after the C_3H_8 and CH_4 co-aromatization reaction, as well as spectra of Zn/HZSM-5 to identify the background. It is clear that the peaks assigned to C_2H_3 and C_2H_4 species are present after the reaction (Fig. 3a), which might originate from the abovementioned double bond species adsorbed on the catalyst surface. The signals at larger mass-to-charge regions are also examined to give more information regarding the bonding between the surface species and the catalytic sites. Among these regions, the peaks located at the molecular mass of 69, 71, 127 and 197 (Fig. 3b-d) stand out as they may originate from $O\text{-}C_4H_5$, $O\text{-}C_4H_7$, $SiAlOC_4H_8$ and $AlO_3ZnC_4H_9$. Notably, the C_4

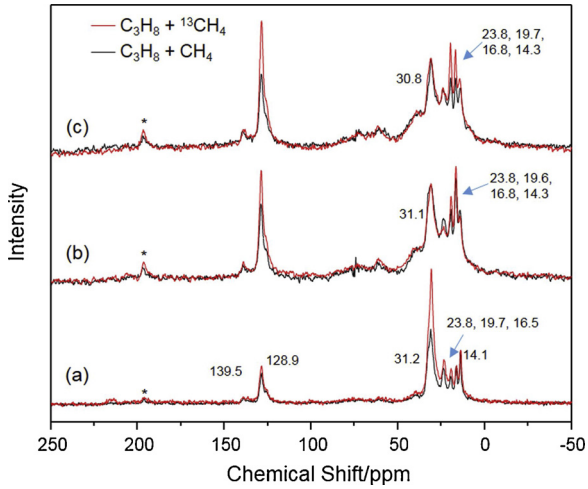

Fig. 2. ^{13}C MAS NMR spectra collected from the catalysts with CH_4/$^{13}CH_4$ and propane co-aromatization products at 5.0 MPa for (a) 15 s (b) 9 min and (c) 20 min. *: spinning sidebands.

species, which might be produced from the reaction between C_3 from C_3H_8 activation and C_1 upon CH_4 activation on the catalyst surface, are clearly observed. As discussed above, in the GC–MS spectra of the products after the reaction for 15 s, C_7H_{16} and C_8H_{18} are observed and may be the reaction intermediates and precursors of aromatic products (Fig. 1 and Figure S2), while the presence of CH_4 in the reaction would promote the formation of C_8H_{18}. This result might be related to the C_4 intermediates formed on the catalyst surface, which may produce C_8 species through coupling of C_4 moieties identified here. The higher carbon number organics are not clearly detected, which might suggest their lower intensities and less significant interaction with the catalytic sites compared with the C_4 species. When looking at the atoms that are bonded to these C_4 species, it is observed that both O and Zn could be the catalytic active sites. The detected $AlO_3ZnC_4H_9$ signal (Fig. 3d) suggests that the Zn oxide species bonded to zeolite oxygen atoms could play a role in the reaction intermediate formation.

3.2.3. Theoretical study of the reaction intermediates

To better understand the reaction intermediates, theoretical calculations were conducted. Prior to its participation in the co-aromatization of methane and propane, a methane molecule is activated by C—H bond cleavage. The CH_3 functional group is then bonded to the catalytic site before its participation in the co-aromatization step. There are several possible sites including Zn and O that may be bonded to the methyl group, which are denoted alkyl and carbenium pathways, respectively [56]. The calculation results (Figure S3 and Table S5) show that the Zn-CH_3 energy is much lower than O-CH_3 in the Zn/HZSM-5 system, with an energy difference as large as 365 kJ/mol. Therefore, the theoretical calculations support that methane is activated through the alkyl pathway over Zn sites, which is consistent with observations of other researchers [28,29,31]. This conclusion also suggests that Zn may play a critical role in methane activation and thus the co-aromatization process.

The SIMS spectra reveal the presence of C_4 species bonded to Zn and O atoms. The peak at *m/z* of 197 is assigned to a fragment with formula $AlO_3ZnC_4H_9$. This may be produced from disparate reaction pathways, shown in Fig. 4. Only the local structure around the organic species is shown in the figure for better illustration. The electrical energies of these structures are tabulated in Table S5. The results show that the structure displayed in Fig. 4a, where a C_4H_9 group is bonded to the Zn atom, is the most stable. In Fig. 4b, a CH_3 is bonded to Zn, while a C_3H_6 group is bonded to an O atom beside the Zn. The energy of this structure is higher than the aforementioned Zn-C_4H_9 structure by 92 kJ/mol. This observation illustrates a plausible reaction pathway leading to the C_4 moiety. CH_3 bonded to Zn upon methane activation may react with C_3H_6 bonded to an oxygen atom, resulting in a C_4H_9 bonded to Zn. In Figs. 4c and 5d, the C_4H_9 group is bonded to an O atom beside Zn or away from Zn, respectively. These structures result in increased energies of 39 and 446 kJ/mol compared to the Zn-C_4H_9 structure shown in Fig. 4a. The comparison of the energies of these structures suggest that the energy of the C_4H_9 group is closely related to the atom it bonds to. Therefore, the Zn-C_4H_9 structure might represent the most favorable pathway, where the C_4H_9 species is stabilized by the Zn site.

In summary, the SSNMR and SIMS studies on the co-aromatization of C_3H_8 and CH_4 over Zn/HZSM-5 have provided some information on the reaction pathway and on intermediates. The methane activation species bonded to Zn react with the C=C moiety formed upon C_3H_8 activation, resulting in reaction intermediates including the C_4 species. Zn sites play a critical role in methane activation and the formation of C_4 species by stabilizing the intermediates. During this process, more

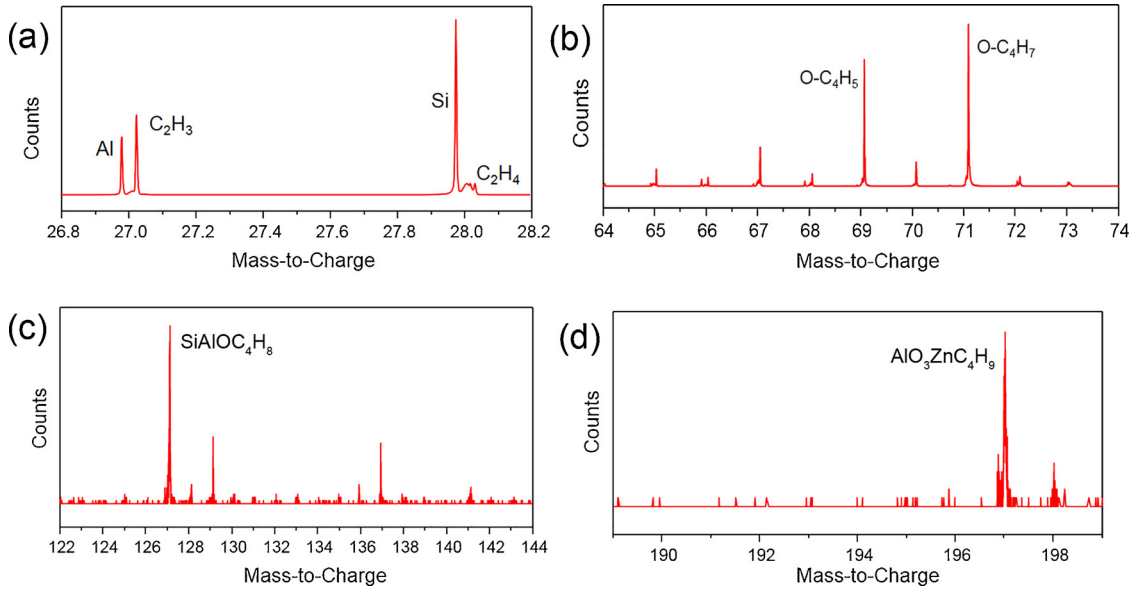

Fig. 3. SIMS spectra of Zn/HZSM-5 upon the co-aromatization reaction between methane and propane at different mass-to-charge ratio regions of 26.8–28.2 (a), 64–74 (b), 122–144 (c) and 189–199 (d).

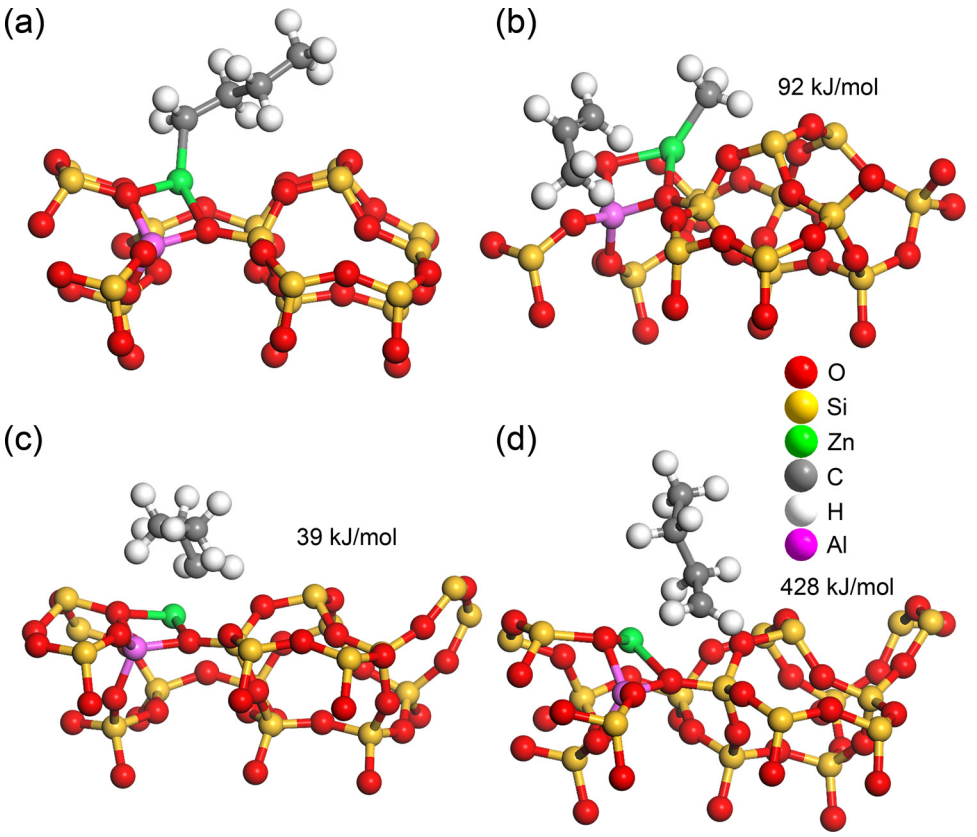

Fig. 4. Structures of Zn/HZSM-5 when the C_4H_9 group is attached to the Zn atom (a), CH_3 is bonded to Zn while C_3H_6 is bonded to the O atom beside Zn (b), the C_4H_9 group is attached to the O atom beside Zn (c) and the C_4H_9 group is attached to an O atom away from Zn (d). The energy increments of (b–d) compared to (a) are listed in the figure.

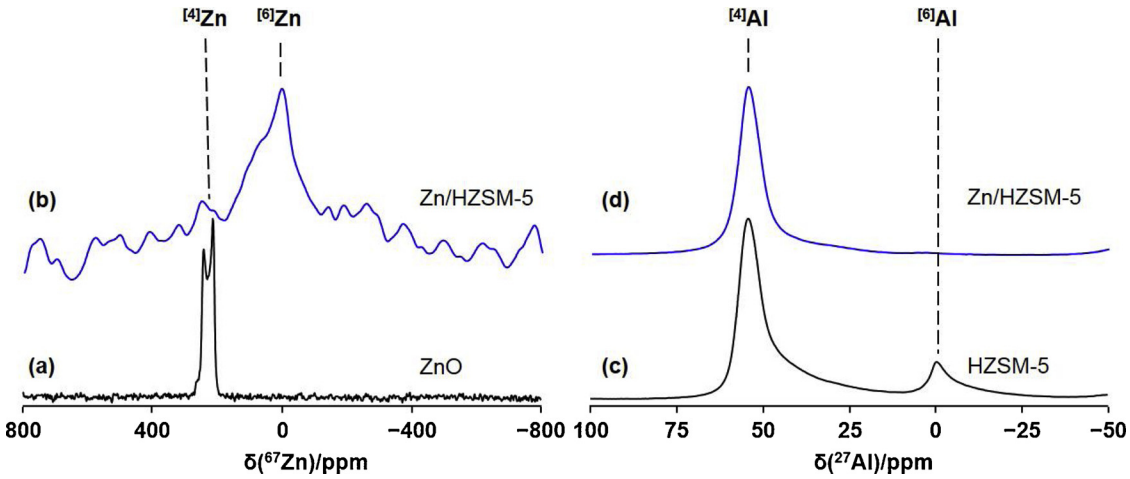

Fig. 5. Static SSNMR ^{67}Zn spectra of ZnO (a) and Zn/HZSM-5 (b) acquired at 21.1 T as well as ^{27}Al MAS NMR spectra of HZSM-5 (c) and of Zn/HZSM-5 (d), acquired at 11.75 T.

OH groups are formed when CH_4 is present, which might be due to proton transfer to the oxygen sites on the zeolite. When the reaction intermediates are further converted to aromatic products, the carbon atom from methane prefers to be incorporated to the benzylic sites initially. As the reaction continues, its incorporation into the phenyl rings is more favorable and consequently greatly enhances phenyl ring formation. When the reaction proceeds further, participation of methane in the substitution groups becomes more significant.

It is challenging to figure out the reason for this altered methane participation pathway due to the complexity of the reaction system. For instance, the presence of aromatics produced in the reaction may affect the activation of methane and its reaction pathway. In methanol-to-olefins reactions, the conversion of methanol is through an indirect hydrocarbon pool mechanism, where hydrocarbon pool molecules such as polymethylbenzenes and polymethylcyclopentenyl are methylated by methanol before the light alkenes are split off. [57] The shift of carbon atoms in the phenyl ring and the side chain is observed in the paring route [58]. Methane participation in this work, such as the methylation reactions, may be affected by the aromatics produced in the reaction in a similar manner. Alkene and alkane products may also impose an effect on the activation of methane and alter its participation pathway. Taking the significant impact of Zn on methane participation into consideration, one conjecture of the methane pathway change is that as the reaction proceeds, the change of the Zn species in the catalyst imposes an effect on the methane participation pathway. Therefore, various characterizations are employed to probe the chemical environment of Zn and its change after the reaction. The characterization results are presented in the following section.

3.3. Evolution of Zn sites

3.3.1. ^{67}Zn and ^{27}Al SSNMR study of the catalysts

The SIMS spectra and theoretical calculation results demonstrate that Zn atoms bonded to the zeolite framework are critical reaction sites for the formation of co-aromatization intermediates. Therefore, to gain further insight into the chemical environment that may impact catalytic performance during the co-aromatization of methane and propane, non-spinning ^{67}Zn SSNMR of ZnO and freshly prepared Zn/HZSM-5 catalyst were acquired at 21.1 T. Fig. 5a and b show ^{67}Zn SSNMR spectra of natural abundance ZnO and Zn/HZSM-5; see Table S6 for parameters derived from this data. The four-coordinate chemical environment of Zn in ZnO (δ_{iso} = 238 ppm) [59,60] shifts to lower frequency upon the incorporation of ZnO into the HZSM-5 zeolite ($\delta_{cgs} \approx$ 30 ppm, where δ_{cgs} describes the center-of-gravity of the observed peak) after calcination. This stark change in chemical shift of ˜ 200 ppm to lower frequency indicates a change in coordination, whereby the detectable Zn/HZSM-5 environments are six-coordinate, with six-coordinate hydrated Zn appearing at approximately 0 ppm (i.e., 1 M solution of $Zn(NO_3)_3$ in water) [66]. The breadth of the spectra also indicate that the nuclear quadrupole coupling constant of Zn/HZSM-5 is larger than that for ZnO, demonstrating that the chemical environment of Zn species in Zn/HZSM-5 is less symmetric than that for ZnO [61]. It has been reported that Zn^{2+} ions at the cation exchange sites, i.e., bonding to the oxygen atoms of ZSM-5 framework (90% ^{67}Zn labeling), results in an increase in ^{67}Zn quadrupolar coupling and a shift to lower frequency, albeit still in the expected four-coordinate region [35]. Our preliminary results for a sample at natural abundance suggest that the local environment of the detectable loaded zinc species are distinct from ZnO, revealing a higher coordination environment with neighboring oxygen species (i.e., H_2O, OX, OH, etc.) [61]. In a 5 wt.%Zn/HZSM-5 with a SiO_2:Al_2O_3 molar ratio of 23:1, the molar ratio between Zn and Al is about 0.56. The study by Yeh et al. [62] shows that each Zn cation displaces one Bronsted acid site at Zn/Al molar ratio below 0.5. The similar Zn/Al molar ratios and preparation methods suggest that Zn atoms are probably at ion-exchange sites in this study. Comparing this result with the ^{27}Al MAS NMR data for both HZSM-5 and Zn/HZSM-5 (Fig. 5c and d) reveals a complementary change whereby HZSM-5 contains both framework ($^{[4]}$Al) and extraframework ($^{[6]}$Al) Al environments, but upon incorporating the ZnO, followed by calcination, virtually no extraframework Al environments are detected. This transformation from $^{[6]}$Al to $^{[4]}$Al environments and corresponding change from $^{[4]}$Zn to $^{[6]}$Zn, may be due to Zn changing the bonding environment of the $^{[6]}$Al upon Zn loading to the ZSM-5 zeolite in the catalyst preparation process. A more thorough study involving isotopically labeled ^{67}Zn would be required to assess whether Zn is incorporated into the zeolite framework or simply located in the pores; unfortunately such an approach is cost prohibitive.

3.3.2. XAS study of the catalysts

X-ray absorption near-edge structure (XANES) of the catalysts is also investigated in this work to further study the chemical environment of Zn species as well as its distribution in the catalyst. Fig. 6 shows the STXM image of the fresh Zn/HZSM-5 particles. The corresponding Zn $L_{3,2}$-edge XANES spectra obtained from the middle and the edge of the particles are also displayed. The Zn $L_{3,2}$-edge monitors the modulation of X-ray absorption coefficient upon excitation of Zn 2p electrons to the previously unoccupied 3d states. The two sets of features, L_3 (˜1025 eV) and L_2 (˜1050 eV) corresponds to electrons from $2p_{3/2}$ and $2p_{1/2}$, respectively. The spectra are normalized to the incident photon flux (I_0) with a unit edge jump. More fluctuation on the L_3 edge adsorption peak is witnessed from the Zn signal on the edge (Fig. 6a) compared with the curve of Zn collected in the middle (Fig. 6b). Besides, the pre-edge and post-edge regions of the curve of Zn in the middle are also more flat compared with that of Zn on the edge of the particles. Therefore, the signal to noise (S/N) ratio of the spectrum collected in a small area in the middle of the particle, where the Zn species is mainly within the inner pores, is significantly improved compared with that collected from the Zn species from a much larger area on the edge of the particles, where there are more Zn species located on or close to the external surface. These observations suggest that the Zn concentration is much higher within inner pores compared with the external surface on the fresh Zn/HZSM-5 catalyst.

XANES spectra at the Zn L edge of the fresh Zn/HZSM-5 and the spent one upon reaction were also collected (Fig. 7) using a Spherical Grating Monochromator (SGM) beamline, which has a more stable beam intensity (I_0) and larger signal acquisition area on the sample. Total fluorescence yield (TFY) signals are generated by the Zn species in the bulk of the sample particles, while the total electron yield (TEY) patterns are obtained from the external surface of the particles. When comparing the absorption threshold (E_0) of Zn on the catalysts with those of Zn, ZnO and $Zn(NO_3)_2{\cdot}6H_2O$, it is observed that the E_0 values of Zn on the catalysts are around 1028 eV, while the E_0 of ZnO is 1030.35 eV, suggesting that the chemical environment of the Zn species loaded on the catalysts is not identical with that of ZnO. It is worth noting that the E_0 value for Zn/HZSM5 is between those for ZnO and $Zn(NO_3)_2{\cdot}6H_2O$, which is consistent with the changes in chemical shift observed in the SSNMR data above (Fig. 5). As these techniques are sensitive to local chemical environments, they both indicate that the Zn coordination environment changes from [4]Zn to [6]Zn when the Zn species is introduced into the Zn/HZSM-5 zeolite.

A closer look at the XANES spectra of the fresh and spent Zn/HZSM-5 reveals that the TEY peak intensities of the spent catalyst after reaction for 15 s remain unchanged, and grow stronger after reaction for 60 min compared with those of the pristine Zn/HZMS-5. The TEY signal of pristine Zn/HZSM-5 is shown as the blue curve. The signal after reaction under a CH_4 environment for 60 min is shown as the red curve. These two curves are overlain to demonstrate the intensity enhancement. This outcome indicates that Zn concentration on the external surface increased after the reaction, i.e., Zn species redistributes towards the external surface.

3.3.3. XPS study of the catalysts

It has been observed that the Zn sites are critical in methane activation and C_4 species formation, and so impose an effect on methane participation in the co-aromatization process. The migration of Zn sites may thus alter the reaction pathway due to the change of chemical environment of Zn. Inspired by the surface Zn concentration change over XANES spectra acquired from the Zn/HZSM-5 before and after the reaction, XPS was employed to characterize the Zn species on the fresh and of spent catalysts to achieve a more accurate measurement of the Zn concentration change on the external surface. The peak intensity due to the Si 2p band is used as the internal standard for the peak intensity quantification of other elements, with the assumption that the Si sites in the framework exposed on the external surface stays intact upon the reaction. The signals collected at Zn 2p, Al 2p and O 1 s regions are displayed in Fig. 8. Clearly the intensity of Zn species increased after reaction for 60 min (Fig. 8a), indicating that some Zn species are transferred to the external surface after the reaction. The concentration of Zn on the external surface is increased by 2.3 times after the reaction based on the pre-calibrated peak area change. The peak locations remain the same upon reaction. These findings show that the oxidation state of the newly transferred Zn species is similar to that of Zn species on the external surface of Zn/HZSM-5 before the reaction. The intensity of O 1 s and Al 2p signals (Fig. 8b and c) for the catalyst are unchanged after the reaction, which is probably because the O and Al sites exposed on the external surface are mainly contributed by the zeolite framework, which are not significantly affected by the reaction. The location of the O 1 s peak is shifted from 530.3 to 530.5 eV after the reaction, suggesting that the chemical environment of oxygen sites are affected by the transferred Zn species, for instance, the bond formation between Zn and O atoms.

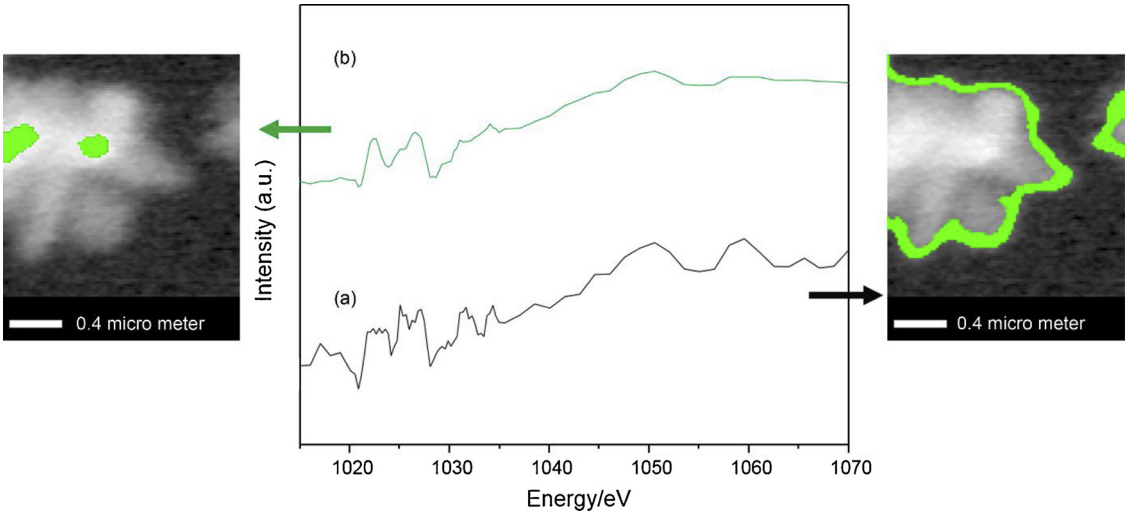

Fig. 6. STXM images of Zn/HZSM-5 particles and the XANES spectra of the Zn species located in the middle (green curve) and on the edge (black curve) of the Zn/HZSM-5 particles (For interpretation of the references to colour in this figure legend, the reader is referred to the web version of this article).

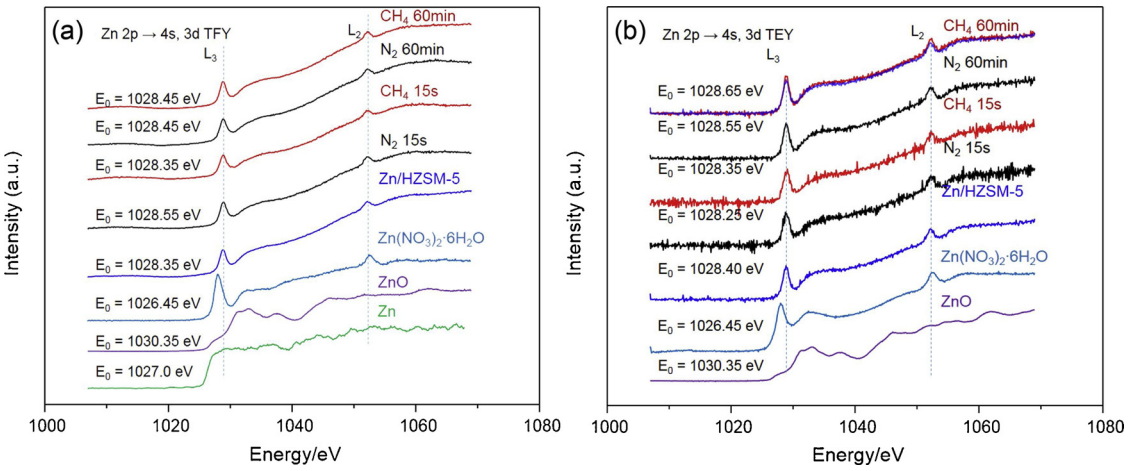

Fig. 7. XANES spectra including the TFY (a) and TEY (b) signals at Zn L-edge of Zn, ZnO, $Zn(NO_3)_2{\cdot}6H_2O$, fresh Zn/HZSM-5 and spent catalysts under 5.0 MPa N_2/CH_4 for 15 s / 60 min at 400 °C. In the upper trace of (b), the TEY spectrum of fresh Zn/HZSM-5 is overlain with that of the spent catalyst after 60 min to demonstrate the peak intensity change.

3.3.4. TEM and EFTEM study of catalysts

The redistribution of Zn species is also evidence by transmission electron microscopy (TEM) accompanied by energy-filtered TEM (EFTEM) images (Fig. 9) obtained from the Zn/HZSM-5 catalysts before and after the reaction. Fig. 9a shows the TEM image of the pristine catalyst, and the corresponding EFTEM image (Fig. 9b). The distribution of light dots on the Zn/HZSM-5 catalyst particle, which demonstrates the presence of Zn, are, with a few exceptions, uniform. After the 60 min co-aromatization reaction the Zn distribution is significantly shifted. Compared with the middle part, the edges of the particles have much stronger Zn signals (Fig. 9c and d). When the zeolite particle is loaded to the TEM sample grid with one face attached to the grid, the edge section of the particle observed on the TEM image contains a larger fraction of external surface areas of the catalyst particles compared with the sections in the middle. Therefore, a brighter edge section due to higher concentration of Zn signal suggests that more Zn is present on the external surface of the Zn/HZSM-5 catalyst particles. The same trend of Zn redistribution is also observed after the reaction for 15 s (Figure S4). The Zn signal increased at the edge of the particles although not as significant as after 60 min. This result indicates that Zn redistribution becomes more significant along with reaction time and facilitates the reaction on the surface.

3.3.5. Theoretical study of Zn distribution

The migration of Zn may be related to the altered reaction pathway since catalytic sites at different locations may tend to catalyze different reaction pathways. The roles of the catalytic sites in inner pore and on external surface of Ag-Ga/HZSM-5 in the co-aromatization of methane and olefins have been investigated [39]. Olefin feedstocks with different sizes and catalysts prepared using various ZSM-5 support materials upon post-synthetic treatment are employed. The concentration of catalytic sites at different locations are manipulated by blocking the inner pore and covering the external surface to directly observe their roles in co-aromatization of methane and olefins. These results suggest that the altered methane participation reaction pathway in the present work may be induced by the Zn migration from the inner pore to the external surface. The catalytic activity of the Zn species in the inner pores and on the external surface is explored through molecular simulation at DFT level. The procedure is described in the supplementary information. In the first scenario, one Zn atom is in the inner pore (10-member ring) and another Zn on the external surface. The energy of the system with one C_4H_9 bonded to the Zn atom, in the inner pore or on the external surface, is calculated (Table S7). The energy difference between the two situations is 42 kJ/mol. In the second scenario, there are two Zn atoms in the inner pores and two Zn atoms on the external surface. The energy difference between the systems with C_4H_9 bonded

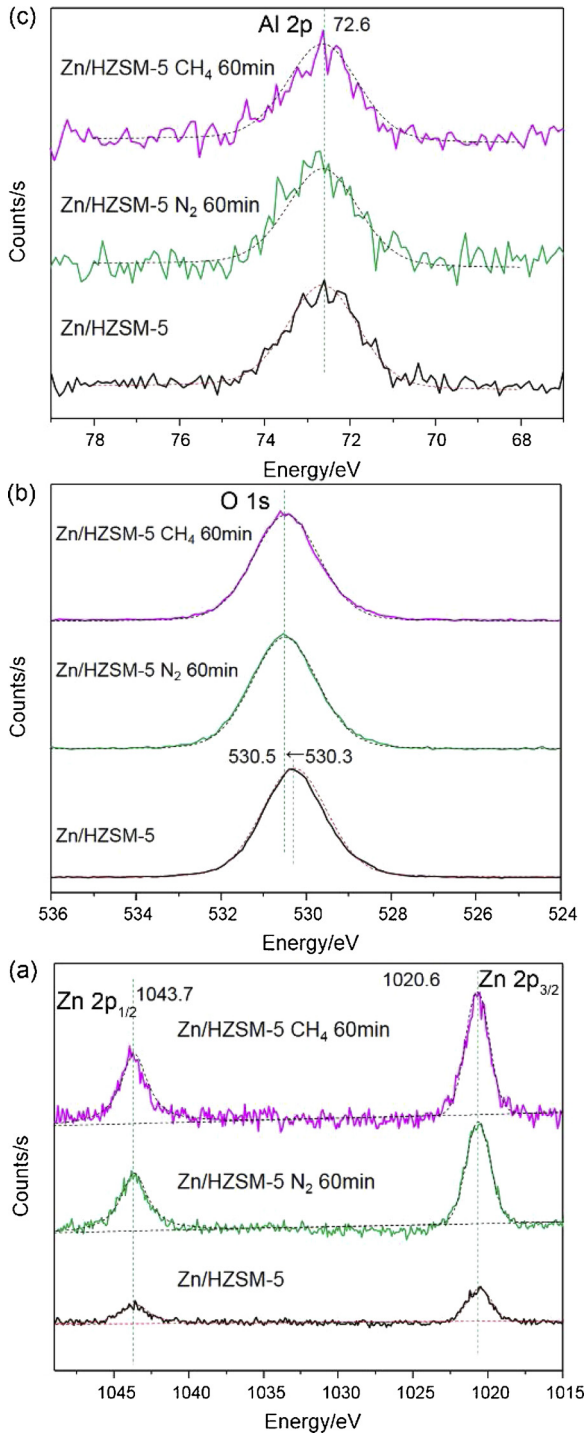

Fig. 8. XPS spectra of Zn/HZSM-5 before and after reactions under N_2/CH_4 for 60 min in the (a) Zn 2p, (b) O 1 s and (c) Al 2p regions.

to inner pore Zn and external surface Zn is 34 kJ/mol. In the third scenario where two catalyst systems with two Zn in the inner pores or on the external surface are built, the energy difference is increased to 71 kJ/mol. The energy changes due to naphthalene ($C_{10}H_8$) and 1-ethyl-3,5-dimethylbenzene, a $C_{10}H_{14}$ molecule with multiple branches, are calculated (Table S8). The energy is lower by 167 and 184 kJ/mol when these molecules are in the inner pores, respectively, suggesting that the product molecules prefer to form over the inner pore Zn sites. It is worth noting that the energy in the presence of naphthalene in the lower than the $C_{10}H_{14}$ counterpart by 17 kJ/mol. These observations demonstrate that the Zn sites in the inner pores are more active in stabilizing the C_4H_9 reaction intermediate and the product molecules. They also favor the formation of $C_{10}H_8$ over $C_{10}H_{14}$, which is in line with the preferred production of naphthalene molecules in the beginning of the reaction.

Theoretical calculations are conducted to gain a better understanding of the Zn distribution in the catalyst. In the aforementioned third structure, the energy difference of the Zn/HZSM-5 frameworks when Zn atoms are located in the inner pores and on the external surface is 55 kJ/mol-Zn. This change is further increased to 105 kJ/mol-Zn when the inner pore Zn atoms are within smaller pores, i.e., 5-member ring (Fig. 10a and b, Table S9). As a consequence, the concentration of Zn in the inner pore is higher in the pristine catalyst. During the reaction, the catalyst is in the environment of CH_4 and C_3H_8 to simplify the system. Theoretical calculation is also employed to explore the effect of these molecules. When CH_4 and C_3H_8 molecules are present around Zn/HZSM-5 the energy difference becomes smaller. Though the energy of the structure with Zn in the inner pores (Fig. 10c) is still lower, the energy difference is only 53 kJ/mol-Zn compared with the external surface counterpart (Fig. 10d) when two CH_4 and two C_3H_8 molecules are in the structure. The energy differences in the presence of one CH_4, two CH_4, and one CH_4 together with one C_3H_8 molecule are also calculated, where narrowed differences are observed in all cases (Table S7). The reduced energy gap between the two Zn site locations under a CH_4 environment may motivate Zn migration from the inner pores, where Zn is very high due to the much lower energy in the beginning, to the external surface during the reaction.

3.4. Methane participation pathway and the effect of Zn distribution

Based on the knowledge obtained in the present work from various characterization techniques including ^{13}C SSNMR and SIMS that investigate the organic intermediates and products, and STXM, XAS, $^{27}Al/^{67}Zn$ SSNMR, TEM, EFTEM and XPS that probe the zeolites chemical environment and spatial distribution of Zn on the catalyst, a hypothesized methane participation pathway in the co-aromatization process with propane, which is affected by Zn redistribution, is proposed in Fig. 11. Due to the complexity of the reaction network, the proposed mechanism only shows one possible reaction route. Upon activation of methane and propane by the Zn/ZSM-5 catalyst, C_4 species are formed at the catalytic sites, which undergo reactions such as dimerization to produce C_8 species and then form single-ring aromatics. The incorporation of methane as methyl groups to phenyl rings is then catalyzed by the catalytic sites, particularly the Zn species located within the inner pores of the catalyst, followed by participation in the phenyl ring formation. The methane incorporation is probably related to the spatial constraint of the inner pores, where a higher concentration of Zn is witnessed compared with the external surface due to the energy difference. This spatial limitation may inhibit methane participation to substitution groups, which results in intermediates and product molecules with much larger molecular sizes. As the reaction proceeds further, some Zn atoms redistribute to the external surface of the Zn/HZSM-5 catalyst since the energy gap between the two Zn locations is smaller in the presence of methane. The Zn species may decrease the Bronsted acid site concentration while increasing the Lewis acid site concentration of the zeolite framework. The migration of Zn from the inner pores to the external surface may thus result in stronger Bronsted acidity in the inner pores and stronger Lewis acidity on the external surface. Besides, the increased Zn concentration on the external surface could enhance methane incorporation in the substitution groups, which has a larger space requirement compared to its incorporation to phenyl rings and benzylic sites. Because of this, the phenyl ring carbon site bonded to the substitution group is not favored by methane participation in these scenarios, which is consistent with observations by the NMR study of ^{13}C isotope labeled samples.

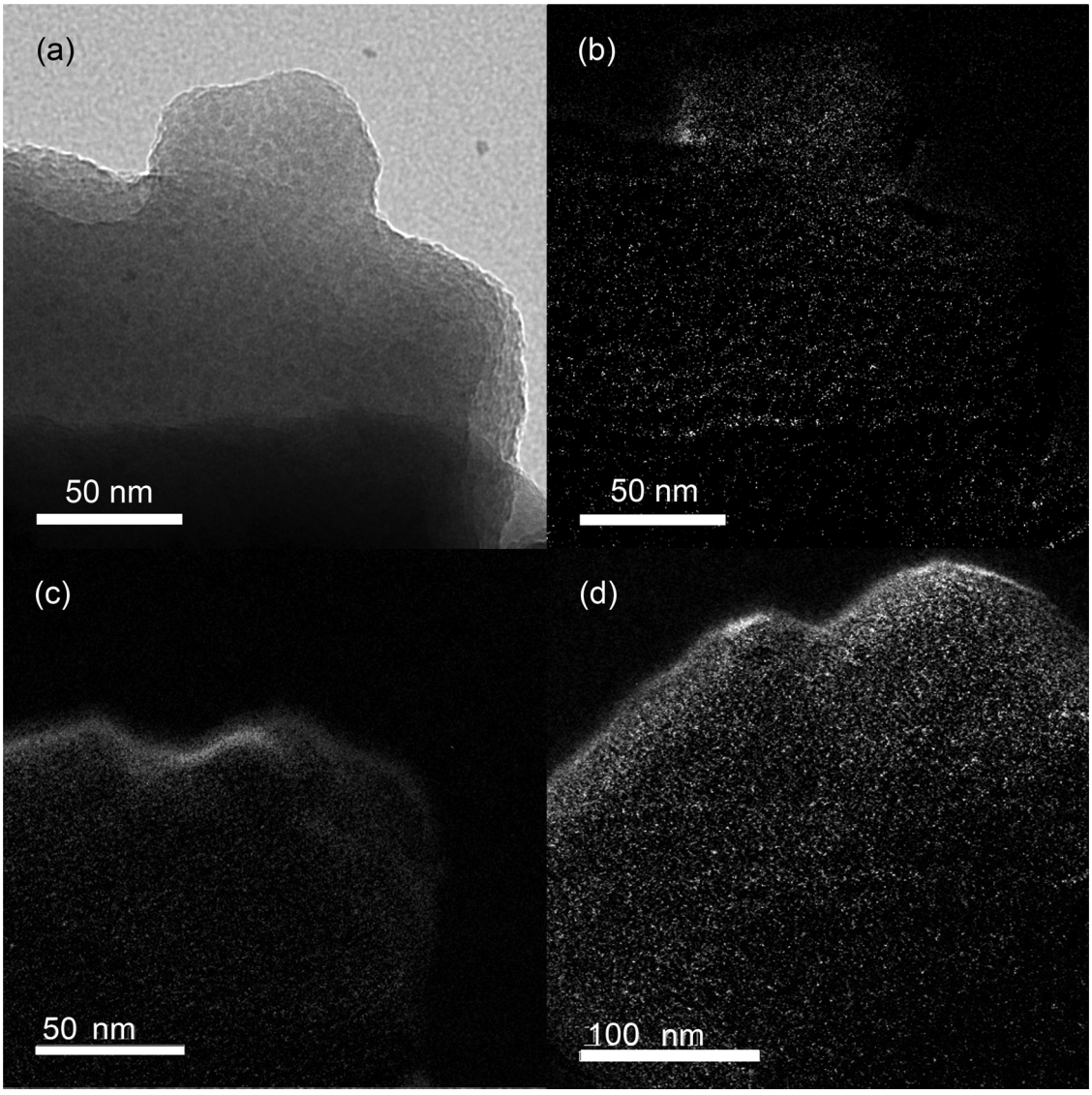

Fig. 9. TEM image of pristine Zn/HZSM-5 catalyst (a) and its EFTEM image (b), and the EFTEM images of the spent catalyst upon the co-aromatization reaction under N_2 (c) and CH_4 (d) environment for 60 min.

4. Conclusions

The presented work investigates the co-aromatization of methane and propane over the Zn/HZSM-5 catalyst at 5.0 MPa and 400 °C, similar to the desired reaction condition for industrial applications. The methane participation demonstrates different reaction pathways and incorporation sites at different stages of the reaction, which might be related to the Zn catalytic site redistribution on the catalyst surface. Initially, methane favors the benzylic sites of the product molecules. Then methane mainly contributes to the phenyl ring formation as the reaction continues. As the reaction proceeds further, the methane incorporation site in the co-aromatization product molecules is on the substitution groups of the formed aromatics. These phenomena are witnessed by GC–MS analysis of the products, and confirmed by a ^{13}C isotope labeling study and SSNMR spectroscopy. The reaction intermediates formed on the catalyst surface are studied by SIMS and theoretical calculations. The reaction between methane and propane in the co-aromatization reaction over Zn/HZSM-5 might be closely related to the reaction between the C_1 and C_3 pieces produced from methane and propane activation. Zn sites bonding to the zeolite framework are critical in the co-aromatization process by stabilizing the intermediates. XAS, XPS, XANES, and ^{67}Zn SSNMR spectroscopies provide further support to the SIMS results on the catalytic zeolite and the importance of Zn. Theoretical calculations predict a lower energy for Zn in the inner pores compared with the external surface in the pristine catalyst, resulting in a higher Zn concentration in the inner pores, which is confirmed by STXM images. The XANES spectra of the pristine catalyst and spent catalysts after the co-aromatization reaction reveal that the Zn concentration on the external surface is increased after the reaction. This phenomenon is further confirmed by EFTEM and XPS analyses, indicating that the Zn species is transferred to the external surface in the reaction and exhibits an interaction with the oxygen sites exposed on the external surface of the zeolite framework, where the space on the external surface is sufficient to hold intermediates and product molecules with large molecular sizes. The migration of Zn is attributed to the decreased energy gap by 52 kJ/mol-Zn between inner pore Zn sites and those on the external surface, which is estimated by DFT calculations. The methane participation pathway is consequently altered to the incorporation to alkyl substitution groups of the formed aromatics at the later stage of the reaction.

Acknowledgements

The authors gratefully acknowledge the financial support from

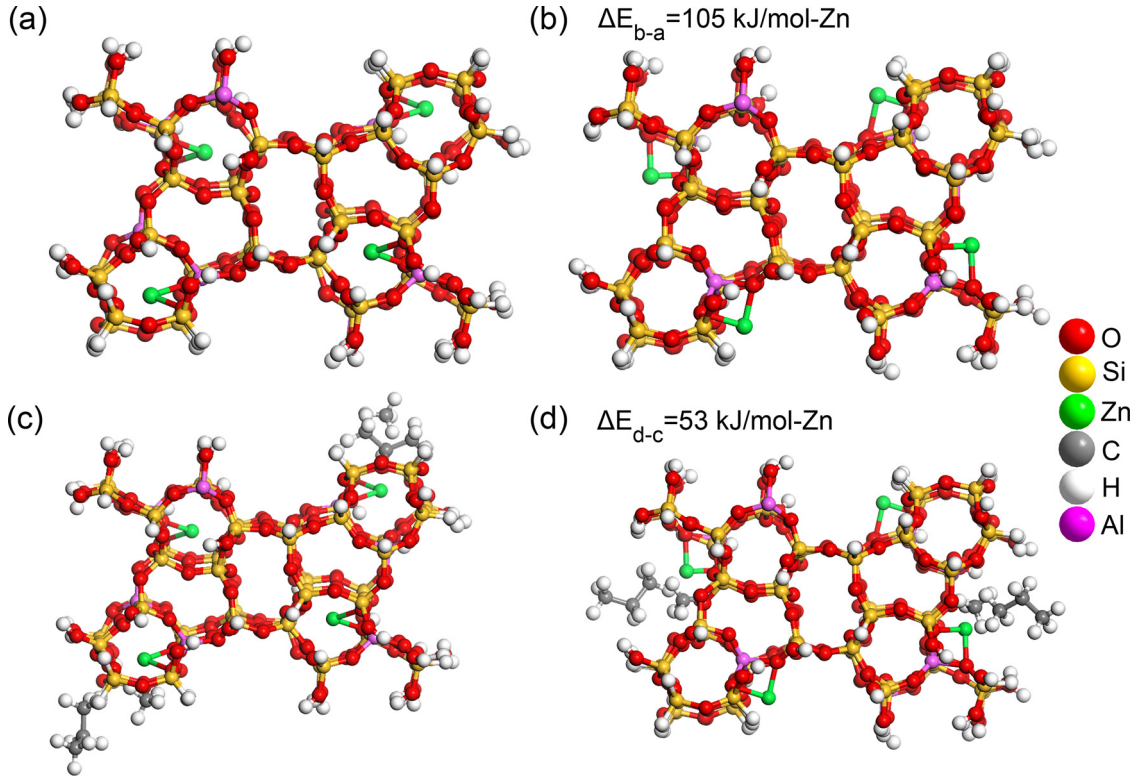

Fig. 10. Structures of Zn/HZSM-5 when Zn atoms are in the inner pores (a) and on the external surface (b) of the ZSM-5 framework. The Zn/HZSM-5 structures in the presence of methane and propane molecules are displayed in (c) and (d).

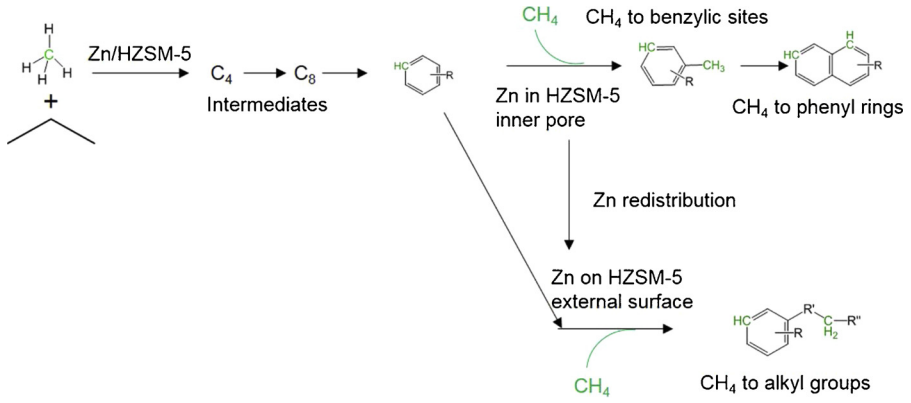

Fig. 11. Proposed reaction pathway for the co-aromatization of methane and propane over Zn/ZSM-5 at 400 °C.

Shandong Chambroad Petrochemicals Co. Ltd. The Natural Sciences and Engineering Research Council (NSERC) of Canada and the University of Alberta are acknowledged for generous research support (VKM). We appreciate the XAS facilities provided by the Canadian Light Source. We thank Dr. Zhiqiang Wang and Dr. Victor V. Terskikh for acquiring the XAS and ^{67}Zn solid-state NMR data, respectively. Access to the 21.1 T NMR spectrometer was provided by the National Ultrahigh-Field NMR Facility for Solids (Ottawa, Canada), a national research facility funded by a consortium of Canadian Universities, supported by the National Research Council Canada and Bruker BioSpin, and managed by the University of Ottawa (http://nmr900.ca).

Appendix A. Supplementary data

Supplementary material related to this article can be found, in the online version, at doi:https://doi.org/10.1016/j.apcatb.2019.03.011.

References

[1] J.H. Lunsford, The catalytic oxidative coupling of methane, Angew. Chem. Int. Ed. 34 (1995) 970–980.
[2] U. Zavyalova, M. Holena, R. Schlögl, M. Baerns, Statistical analysis of past catalytic data on oxidative methane coupling for new insights into the composition of high-performance catalysts, ChemCatChem 3 (2011) 1935–1947.
[3] Z.J. Zhao, A. Kulkarni, L. Vilella, J.K. Nørskov, F. Studt, Theoretical insights into the selective oxidation of methane to methanol in copper-exchanged mordenite, ACS Catal. 6 (2016) 3760–3766.
[4] K. Narsimhan, V.K. Michaelis, G. Mathies, W.R. Gunther, R.G. Griffin, Y. Roman-Leshkov, Methane to acetic acid over cu-exchanged zeolites: mechanistic insights from a site-specific carbonylation reaction, J. Am. Chem. Soc. 137 (2015) 1825–1832.
[5] F. Mudu, U. Olsbye, B. Arstad, S. Diplas, Y. Li, H. Fjellvåg, Aluminium substituted lanthanum based perovskite type oxides, non-stoichiometry and performance in methane partial oxidation by framework oxygen, Appl. Catal. A Gen. 523 (2016) 171–181.
[6] V.T.T. Ha, A. Sarıoğlan, A. Erdem-Şenatalar, Y.B. Taârit, An EPR and NMR study on Mo/HZSM-5 catalysts for the aromatization of methane: investigation of the location of the pentavalent molybdenum, J. Mol. Catal. A Chem. 378 (2013) 279–284.
[7] X. Guo, G. Fang, G. Li, H. Ma, H. Fan, L. Yu, C. Ma, X. Wu, D. Deng, M. Wei, D. Tan,

R. Si, S. Zhang, J. Li, L. Sun, Z. Tang, X. Pan, X. Bao, Direct, nonoxidative conversion of methane to ethylene, aromatics, and hydrogen, Science 344 (2014) 616–619.
[8] T.V. Choudhary, E. Aksoylu, D. Wayne Goodman, Nonoxidative activation of methane, Catal. Rev. 45 (2003) 151–203.
[9] P. Tang, Q. Zhu, Z. Wu, D. Ma, Methane activation: the past and future, Energy Env. Sci. 7 (2014) 2580–2591.
[10] J. Xue, Y. Chen, Y. Wei, A. Feldhoff, H. Wang, J. Caro, Gas to liquids: natural gas conversion to aromatic fuels and chemicals in a hydrogen-permeable ceramic hollow Fiber membrane reactor, ACS Catal. 6 (2016) 2448–2451.
[11] V. Abdelsayed, D. Shekhawat, M.W. Smith, Effect of Fe and Zn promoters on Mo/HZSM-5 catalyst for methane dehydroaromatization, Fuel 139 (2015) 401–410.
[12] J.J. Spivey, G. Hutchings, Catalytic aromatization of methane, Chem. Soc. Rev. 43 (2014) 792–803.
[13] T. Baba, Y. Abe, Metal cation–acidic proton bifunctional catalyst for methane activation: conversion of $^{13}CH_4$ in the presence of ethylene over metal cations-loaded H-ZSM-5, Appl. Catal. A Gen. 250 (2003) 265–270.
[14] O.A. Anunziata, G.V.G. Mercado, L.B. Pierella, Improvement of methane activation using *n*-Hexane as Co-reactant over Zn/HZSM-11 zeolite, Catal. Commun. 5 (2004) 401–405.
[15] P. He, W. Shan, Y. Xiao, H. Song, Performance of Zn/ZSM-5 for in situ catalytic upgrading of pyrolysis bio-oil by methane, Top. Catal. 59 (2015) 86–93.
[16] V.R. Choudhary, K.C. Mondal, S.A.R. Mulla, Simultaneous conversion of methane and methanol into gasoline over bifunctional Ga-, Zn-, in-, and/or Mo-Modified ZSM-5 zeolites, Angew. Chem. Int. Ed. 117 (2005) 4455–4459.
[17] A. Wang, P. He, M. Yung, H. Zeng, H. Qian, H. Song, Catalytic Co-aromatization of ethanol and methane, Appl. Catal. B Env. 198 (2016) 480–492.
[18] P. He, L. Zhao, H. Song, Bitumen partial upgrading over Mo/ZSM-5 under methane environment: methane participation investigation, Appl. Catal. B Env. 201 (2017) 438–450.
[19] V.R. Choudhary, A.K. Kinage, T.V. Choudhary, Low-Temperature Nonoxidative Activation of Methane over H-Galloaluminosilicate (MFI) Zeolite, Science 275 (1997) 1286–1288.
[20] H. Xiao, J. Zhang, X. Wang, Q. Zhang, H. Xie, Y. Han, Y. Tan, A highly efficient Ga/ZSM-5 catalyst prepared by formic acid impregnation and in situ treatment for propane aromatization, Catal. Sci. Technol. 5 (2015) 4081–4090.
[21] Vd.O. Rodrigues, F.J. Vasconcellos, Ad.C. Faro Jr., Mechanistic studies through H–d exchange reactions: propane Aromatization in HZSM5 and Ga/HZSM5 catalysts, J. Catal. 344 (2016) 252–262.
[22] A. Bhan, S. Hsu, G. Blau, J. Caruthers, V. Venkatasubramanian, W. Delgass, Microkinetic modeling of propane aromatization over HZSM-5, J. Catal. 235 (2005) 35–51.
[23] A. Bhan, W. Nicholas Delgass, Propane aromatization over HZSM-5 and Ga/HZSM-5 catalysts, Catal. Rev. 50 (2008) 19–151.
[24] T. Gong, L. Qin, J. Lu, H. Feng, ZnO Modified ZSM-5 and Y zeolites fabricated by atomic layer deposition for propane conversion, Phys. Chem. Chem. Phys. 18 (2016) 601–614.
[25] J.A. Biscardi, G.D. Meitzner, E. Iglesia, Structure and density of active Zn species in Zn/H-ZSM5 propane aromatization catalysts, J. Catal. 179 (1998) 192–202.
[26] T.E. Tshabalala, M.S. Scurrell, Aromatization of *n*-Hexane over Ga, Mo and Zn modified H-ZSM-5 zeolite catalysts, Catal. Commun. 72 (2015) 49–52.
[27] A.A. Gabrienko, S.S. Arzumanov, D. Freude, A.G. Stepanov, Propane aromatization on Zn-Modified zeolite BEA studied by solid-state NMR in situ, J. Phys. Chem. C 114 (2010) 12681–12688.
[28] J. Xu, A. Zheng, X. Wang, G. Qi, J. Su, J. Du, Z. Gan, J. Wu, W. Wang, F. Deng, Room temperature activation of methane over Zn modified H-ZSM-5 zeolites: insight from solid-state NMR and theoretical calculations, Chem. Sci. 3 (2012) 2932.
[29] Y.G. Kolyagin, I.I. Ivanova, V.V. Ordomsky, A. Gedeon, Y.A. Pirogov, Methane activation over Zn-Modified MFI zeolite: NMR evidence for Zn-Methyl surface species formation, J. Phys. Chem. C 112 (2008) 20065–20069.
[30] J.F. Wu, S.M. Yu, W.D. Wang, Y.X. Fan, S. Bai, C.W. Zhang, Q. Gao, J. Huang, W. Wang, Mechanistic insight into the formation of acetic acid from the direct conversion of methane and carbon dioxide on zinc-modified H-ZSM-5 zeolite, J. Am. Chem. Soc. 135 (2013) 13567–13573.
[31] M.V. Luzgin, V.A. Rogov, S.S. Arzumanov, A.V. Toktarev, A.G. Stepanov, V.N. Parmon, Understanding methane aromatization on a Zn-modified high-silica zeolite, Angew. Chem. Int. Ed. 47 (2008) 4559–4562.
[32] A.A. Gabrienko, S.S. Arzumanov, A.V. Toktarev, I.G. Danilova, I.P. Prosvirin, V.V. Kriventsov, V.I. Zaikovskii, D. Freude, A.G. Stepanov, Different efficiency of $Zn^{2+}$and ZnO species for methane activation on Zn-modified zeolite, ACS Catal. 7 (2017) 1818–1830.
[33] C.K. Brozek, V.K. Michaelis, T.C. Ong, L. Bellarosa, N. Lopez, R.G. Griffin, M. Dinca, Dynamic DMF binding in MOF-5 enables the formation of metastable cobalt-substituted MOF-5 analogues, ACS Cent. Sci. 1 (2015) 252–260.
[34] A. Sutrisno, V.V. Terskikh, Q. Shi, Z. Song, J. Dong, S.Y. Ding, W. Wang, B.R. Provost, T.D. Daff, T.K. Woo, Y. Huang, Characterization of Zn-containing metal-organic frameworks by solid-state ^{67}Zn NMR spectroscopy and computational modeling, Chem. Eur. J. 18 (2012) 12251–12259.
[35] G. Qi, Q. Wang, J. Xu, J. Trebosc, O. Lafon, C. Wang, J.P. Amoureux, F. Deng, Synergic effect of active sites in zinc-modified ZSM-5 zeolites as revealed by high-field solid-state NMR spectroscopy, Angew. Chem. Int. Ed. 55 (2016) 15826–15830.
[36] P. He, B.E.G. Lucier, V.V. Terskikh, Q. Shi, J. Dong, Y. Chu, A. Zheng, A. Sutrisno, Y. Huang, Spies within metal-organic frameworks: investigating metal centers using solid-state NMR, J. Phys. Chem. C 118 (2014) 23728–23744.
[37] N. Kosinov, F.J.A.G. Coumans, E.A. Uslamin, A.S.G. Wijpkema, B. Mezari, E.J.M. Hensen, Methane dehydroaromatization by Mo/HZSM-5: mono- or bifunctional catalysis? ACS Catal. 7 (2017) 520–529.
[38] W. Ding, G.D. Meitzner, E. Iglesia, The effects of silanation of external acid sites on the structure and catalytic behavior of Mo/H-ZSM5, J. Catal. 206 (2002) 14–22.
[39] P. He, J. Jarvis, S. Meng, A. Wang, S. Kou, R. Gatip, M. Yung, L. Liu, H. Song, Co-aromatization of methane with olefins: the role of inner pore and external surface catalytic sites, Appl. Catal. B Env. 234 (2018) 234–246.
[40] G. Chen, Y. Zhao, L. Shang, G. Waterhouse, X. Kang, L. Wu, C. Tung, T. Zhang, Recent advances in the synthesis, characterization and application of Zn^+ -containing heterogeneous catalysts, Adv. Sci. 3 (2016) 1500424.
[41] H. Berndt, G. Lietz, B. Lücke, J. Völter, Zinc promoted H-ZSM-5 catalysts for conversion of propane to aromatics I. Acidity and activity, Appl. Catal. A Gen. 146 (1996) 351–363.
[42] M.W. Schreiber, C.P. Plaisance, M. Baumgärtl, K. Reuter, A. Jentys, R. Bermejo-Deval, J.A. Lercher, Lewis−Brønsted Acid Pairs in Ga/H-ZSM-5 to catalyze Dehydrogenation of Light Alkanes, J. Am. Chem. Soc. 140 (2018) 4849–4859.
[43] N.M. Schweitzer, B. Hu, U. Das, H. Kim, J. Greeley, L.A. Curtiss, P.C. Stair, J.T. Miller, A.S. Hock, Propylene hydrogenation and propane dehydrogenation by a single-site Zn^{2+} on silica catalyst, ACS Catal. 4 (2014) 1091–1098.
[44] J.I. Goldstein, D.E. Newbury, J.R. Michael, N.M. Ritchie, J.J. Scott, D.C. Joy, Scanning Electron Microscopy and X-Ray Microanalysis Fourth Edition, Springer, 2017.
[45] W.L. Earl, D.L. Vanderhart, Measurement of ^{13}C chemical shifts in solids, J. Magn. Reson. 48 (1982) 35–54.
[46] R.K. Harris, E.D. Becker, NMR nomenclature: nuclear spin properties and conventions for chemical Shifts-IUPAC recommendations, J. Magn. Reson. 156 (2002) 323–326.
[47] G.E. Maciel, L. Simeral, J.J.H. Ackerman, Effect of complexation of zinc (II) on zinc-67 chemical shifts, J. Phys. Chem. 81 (1977) 263–267.
[48] Z. Wang, J. Wang, T.K. Sham, S. Yang, Tracking the Interface of an Individual ZnS/ZnO Nano-Heterostructure, J. Phys. Chem. C 116 (2012) 10375–10381.
[49] T. Regier, J. Krochak, T.K. Sham, Y.F. Hu, J. Thompson, R.I.R. Blyth, Performance and capabilities of the canadian dragon: the SGM beamline at the canadian light source, Nucl. Instrum. Methods Phys. Res. Sect. A 582 (2007) 93–95.
[50] S. Subramanian, G. Clark, K. Ly, T. Chrastecky, Energy-filtered transmission Electron microscopy (EFTEM) of semiconductor devices, Electron. Device Failure Anal. 13 (2010) 20–28.
[51] A.D. Becke, Density-functional exchange-energy approximation with correct asymptotic behavior, Phys. Rev. A 38 (1988) 3098–3100.
[52] J.P. Perdew, K. Burke, M. Ernzerhof, Generalized gradient approximation made simple, Phys. Rev. Lett. 77 (1996) 3865–3868.
[53] J. Ohara, Y. Kim, S. Yanagisawa, Y. Morikawa, M. Kawai, Role of molecular orbitals near the fermi level in the excitation of vibrational modes of a single molecule at a scanning tunneling microscope junction, Phys. Rev. Lett. 100 (2008) 136104.
[54] J.G. Fripiat, F. Berger-Andre, J.M. Andre, E.G. Derouane, Non-empirical quantum mechanical calculations on pentasil-type zeolites, Zeolites 3 (1983) 306–310.
[55] E. Pretsch, P. Buhlmann, M. Badertscher, Structure Determination of Organic Compounds. Tables of Spectral Data, Fourth, Revised and Enlarged Edition ed. Springer-Verlag, Berlin Heidelberg, 2009.
[56] M.V. Luzgin, A.A. Gabrienko, V.A. Rogov, A.V. Toktarev, V.N. Parmon, A.G. Stepanov, The "Alkyl" and "Carbenium" pathways of methane activation on Ga-modified zeolite BEA:^{13}C solid-state NMR and GC-MS study of methane aromatization in the presence of higher alkane, J. Phys. Chem. C 114 (2010) 21555–21561.
[57] C. Li, C. Paris, J. Martinez-Triguero, M. Boronat, M. Moliner, A. Corma, Synthesis of reaction-adapted zeolites as methanol-to-Olefins catalysts with mimics of reaction intermediates as organic structure-directing agents, Nat. Catal. 1 (2018) 547–554.
[58] S. Xu, A. Zheng, Y. Wei, J. Chen, J. Li, Y. Chu, M. Zhang, Q. Wang, Y. Zhou, J. Wang, F. Deng, Z. Liu, Direct observation of cyclic carbenium ions and their role in the-catalytic cycle of the methanol-to-Olefin reaction over chabazite zeolites, Angew. Chem. Int. Ed. 52 (2013) 11564–11568.
[59] S.F. Dec, M.F. Davis, G.E. Maciel, C.E. Bronnimann, J.J. Fitzgerald, S.S. Han, Solid-state multinuclear NMR studies of ferroelectric, piezoelectric, and related materials, Inorg. Chem. 32 (1993) 955–959.
[60] T.J. Bastow, S.N. Stuart, NMR Study of the Zinc Chalcogenides (ZnX, X = O, S, Se, Te), Phys. Status Solidii B 145 (1988) 719–728.
[61] S. Sham, G. Wu, Zinc-67 NMR of zinc sites with tetrahedral and octahedral oxygen, nitrogen and sulfur ligands, Can. J. Chem. 77 (1999) 1782–1787.
[62] Y. Yeh, S. Zhu, P. Staiber, R.F. Lobo, R.J. Gorte, Zn-promoted H-ZSM-5 for endothermic reforming of *n*-Hexane at high pressures, Int. Eng. Chem. Res. 55 (2016) 3930–3938.